HHS Public Access

Author manuscript

Nanomedicine. Author manuscript; available in PMC 2018 April 01.

Published in final edited form as:

Nanomedicine. 2017 April ; 13(3): 909–920. doi:10.1016/j.nano.2016.12.005.

Fluorescent nanodiamonds engage innate immune effector cells: a potential vehicle for targeted anti-tumor immunotherapy

Lorena P. Suarez-Kelly, M.D.[a,*], **Amanda R. Campbell, Ph.D.**[a,b,*], **Isaac V. Rampersaud**[c], **Ambika Bumb, Ph.D.**[d], **Min S. Wang, Ph.D.**[d], **Jonathan P. Butchar, Ph.D.**[e], **Susheela Tridandapani, Ph.D.**[e], **Lianbo Yu, Ph.D.**[f], **Arfaan A. Rampersaud, Ph.D.**[c], and **William E. Carson III, M.D.**[a,g,+]

[a]The Arthur G. James Comprehensive Cancer Center and Solove Research Institute, The Ohio State University, Columbus, OH 43210, USA

[b]Medical Scientist Training Program and Biomedical Sciences Graduate Program, The Ohio State University, Columbus, OH 43210, USA

[c]Columbus NanoWorks, Inc., 1507 Chambers Road, Columbus, OH 43212, USA

[d]Bikanta Inc., Molecular Foundry, 1 Cyclotron Road Building 67, Berkeley, CA 94720, USA

[e]Division of Pulmonary, Allergy, Critical Care and Sleep Medicine, Department of Internal Medicine, The Ohio State University, Columbus, OH 43210, USA

[f]Department of Biomedical Informatics, The Ohio State University, Columbus, OH 43210, USA

[g]Department of Surgery, The Ohio State University, Columbus, OH 43210, USA

Abstract

Fluorescent nanodiamonds (FNDs) are nontoxic, infinitely photostable, and emit fluorescence in the near infrared region. Natural killer (NK) cells and monocytes are part of the innate immune system and are crucial to the control of carcinogenesis. FND-mediated stimulation of these cells may serve as a strategy to enhance anti-tumor activity. FNDs were fabricated with a diameter of 70±28 nm. Innate immune cell FND uptake, viability, surface marker expression, and cytokine production were evaluated *in vitro*. Evaluation of fluorescence emission from the FNDs was conducted in an animal model. *In vitro* results demonstrated that treatment of immune cells with

[+]**Corresponding Author**: William E. Carson III, MD, FACS, The Arthur G. James Comprehensive Cancer Center and Richard J. Solove Research Institute, The Ohio State University, N924 Doan Hall 410 W. 10th Ave, Columbus, OH 43210-1228. E-mail: william.carson@osumc.edu, Office Phone: (614) 293-6306, FAX: (614) 293-3465.

[*]These authors have contributed equally to this work.

Disclosures: Authors from Bikanta and Columbus NanoWorks commercially develop nanodiamond imaging technologies. All other authors declare no financial or non-financial competing interests and also declare no spouses, partners, or children with relationships with commercial entities that might have interest in the submitted work.

Prior Presentations: Abstracts of this work were presented at the Annual Presidential Symposium of the Columbus Surgical Society in Columbus, OH (2016, February) and at the Society of Surgical Oncology 69th Annual Cancer Symposium in Boston, MA (2016, March). This manuscript, or any part of it, has not been published and will not be submitted elsewhere for publication while being considered by the journal Nanomedicine: Nanotechnology, Biology, and Medicine.

FNDs resulted in significant dose-dependent FND uptake, no compromise in cell viability, and immune cell activation. FNDs were visualized in an animal model. Hence, FNDs may serve as novel agents with “track and trace” capabilities to stimulate innate immune cell anti-tumor responses, especially as FNDs are amenable to surface-conjugation with immunomodulatory molecules.

GRAPHICAL ABSTRACT

Fluorescent nanodiamonds (FNDs) are a unique tool that may be employed in the treatment of cancer. High-energy electron beams are employed to introduce nitrogen vacancy centers within the diamond lattice to yield infinitely photostable near-infrared fluorescence. Upon treatment of immune cells with biocompatible FNDs, FNDs are taken up and may be visualized within the cytoplasm by flow cytometry and confocal microscopy. FNDs present an extensive, modifiable surface area and may serve as a vector for targeted delivery of immunomodulatory agents to promote immune cell effector functions in the fight against cancer.

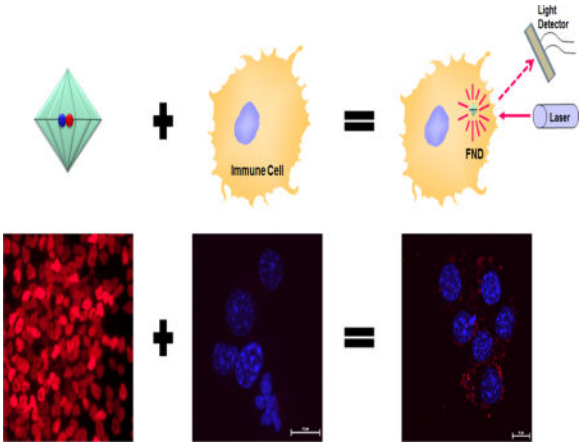

Keywords

Fluorescence; Nanodiamonds; Immunotherapy; Natural killer cells; Monocytes

BACKGROUND

Fluorescent nanodiamonds (FNDs) are unique, multifunctional reagents that may be employed in cancer immunotherapy and other biomedical applications. The generation of nitrogen vacancy (NV)-centers within the diamond lattice endows nanodiamonds with fluorescent properties.[1–3] FNDs containing NV-centers are nontoxic, biocompatible nanomaterials that emit strong fluorescence in the near-infrared (NIR) region, remain photostable in the presence of intense laser excitation (>1 GW/cm^2), and exhibit excellent *in vivo* stability.[4–7] Additionally, FNDs present an extensive, modifiable surface area owing to their faceted architecture.[6,8]

The versatile surface of FNDs may be functionally modified. Some functional modification techniques include coating FNDs with biocompatible molecules, such as polyethylene glycol, glycidol or cellobiose, which may be further conjugated for targeted drug delivery

applications.[9–11] Importantly, FND surface functionalization may be used as a potential therapeutic anti-tumor strategy. Emerging therapeutic delivery platforms displaying peptides, proteins, and nucleic acids are being developed and provide FNDs with a broad range of future therapeutic options.[12–15] Therefore, FNDs have the potential to be coated with biocompatible chemicals, conjugated to antibodies or other immunomodulatory agents, and thereby targeted to innate immune cells to promote anti-tumor activity.[9–12,16–18]

Innate immune cells contribute to cancer immunosurveillance through recognition and elimination of developing tumors. Monocytes and natural killer (NK) cells are key contributors to this line of defense. Monocytes are phagocytic cells that target and kill opsonized cells.[19–21] NK cells are non-MHC-restricted cytotoxic lymphocytes that have the ability to lyse transformed cells without prior sensitization.[22,23] Upon activation, these cells secrete several immune stimulatory cytokines (e.g., TNF-α and IL-12 by monocytes/macrophages and IFN-γ by NK cells) and upregulate expression of surface molecules indicative of activation (e.g., HLA-DR and CD86 on monocytes and NKG2D and CD69 on NK cells).[24–27] These responses not only mediate direct anti-tumor activity but also promote the recruitment of adaptive immune cells, which further enhances the anti-tumor immune response.[20–22,28–30] Thus, immunotherapeutic strategies that target monocytes and NK cells to promote their effector functions may provide a mechanism to modulate the tumor microenvironment and inhibit tumorigenesis.

With the knowledge that the immune system shapes the course of tumor progression, scientists in the growing field of cancer immunotherapy have aspired to identify immune-modulatory agents to harness the power of the immune system for the treatment of cancer. In the present study, it was hypothesized that FNDs may serve as vectors for targeted immune cell activation to promote anti-tumor activity. To address this question, it was important to first evaluate direct immune cell uptake, biocompatibility, and immunostimulation mediated by unconjugated FNDs prior to examining further biomedical applications. Therefore, we have characterized the behavior of monocytes and NK cells following exposure to unconjugated FNDs through evaluation of cellular uptake, FND localization, cell viability and effects on immune cell activation. The findings presented herein support future investigation into novel therapeutic applications utilizing FNDs. Notably, this study confirms that innate immune cells will take up FNDs with no compromise in cell viability and result in stimulation of pro-inflammatory responses. Hence, these results support the notion that FNDs may serve as novel agents to stimulate innate immune cell anti-tumor responses.

METHODS

Reagents and Cell Lines

Murine macrophage cell line, RAW264.7, was obtained from American Type Culture Collection (Manassas, VA). Human natural killer cell (NKL) cell line was provided by Dr. Michael A. Caligiuri at The Ohio State University.

FND Preparation

Columbus Nanoworks, Inc. (Columbus, OH) generated FNDs from micron-sized, high pressure, high temperature diamonds that were then milled to nanoscale size and cleaned with concentrated sulfuric acid and nitric acid as previously described.[31] The FNDs generated in this study were uncoated, non-functionalized, and not activated.

FND Characterization

Samples were prepared by depositing 0.0005% (w/w) FNDs on a coverslip and drying in a vacuum oven for 2 hours. Scanning electron microscopy (SEM) images were acquired on a field emission scanning electron microscope (Zeiss Ultra 55) operating at 5 kV and a working distance of 7.9 mm. Size characterization was performed from the SEM images (n = 168) using Image J. The fluorescence emission spectrum was obtained using a Horiba ARAMIS Raman upright microscope (50× objective) and a 532 nm excitation laser. Confocal microscopy images were collected on an Olympus FV1000-Filter Confocal System using a 543 nm excitation laser and corresponding 655/55 nm barrier filters.

Isolation of Human NK Cells and Monocytes

Peripheral blood mononuclear cells (PBMC) and NK cells were isolated from healthy donor leukopacks (American Red Cross, Columbus, OH) as previously described.[32] For NK cell isolation, PBMC were incubated for 30 minutes with RosetteSep Human NK Cell Enrichment Cocktail (Immunodensity Negative Selection Cocktail, Stem Cell Technologies, Vancouver, BC). Ficoll hypaque density gradient centrifugation was performed and PBMC and NK cells were collected. NK cells procured in this manner were confirmed to be greater than 95% pure by flow cytometric analysis according to their CD56 surface marker expression. For monocyte isolation, PBMC were added to 6-well plastic plates and allowed to adhere for 24 hours prior to washing and harvesting the monolayer. Monocytes procured in this manner were confirmed to be greater than 94% pure by flow cytometric analysis according to their CD14 surface marker expression. Immune cells were cultured in RPMI-1640 medium supplemented with 10% heat-inactivated pooled human AB serum (C-six Diagnostics; Germantown, WI), 100 units/ml of penicillin, 100 μg/ml of streptomycin, and 0.25 μg/ml of amphotericin B (10% HAB medium).

In vitro FND Treatment Assays

RAW264.7 cells, monocytes, NKL cells and NK cells were added to 24-well flat-bottom plates at a concentration of 1×10^6 cells/well in 10% HAB medium alone (untreated control) or medium supplemented with FNDs and cultured at 37°C. For functional analyses of FND-treated NK cells, additional treatment groups stimulated with 1 μg/ml of IL-12 were evaluated. Cell-free culture supernatants or cells were collected for analysis.

Flow Cytometry

Flow cytometry was performed on a LSR II flow cytometer (BD Biosciences, San Jose, CA). Monocytes were labeled with a CD14-allphycocyanin (APC) monoclonal-antibody (mAb) (Beckman Coulter, Brea, CA) and NK cells were labeled with a CD56/NKH1-RD1-phycoerythrin (PE) mAb (Beckman Coulter, Brea, CA). Cells were gated based on forward

laser light scatter (FS) and side laser light scatter (SS) and monocyte and NK cell populations were gated according to their CD14 or CD56 surface marker expression, respectively. Purity greater than 94% for monocytes and 95% for NK cells was confirmed via flow cytometric analysis (FlowJo, Ashland, OR). Immune cell FND uptake was evaluated by changes in FS, SS, and NIR fluorescence measured in the PE-Cyanin 5.1 channel compared to untreated controls. Monocyte surface marker expression was examined via CD86-PE and HLA-DR-APC mAb (BD Pharmingen, San Jose, CA) staining, as previously described.[33] NK cell surface marker expression was examined via CD69-PE and NKG2D-APC mAb (BD Pharmingen, San Jose, CA) staining.[33] Percentage of positively staining cells, mean fluorescence intensity (MFI), and fold-change in fluorescence compared to untreated controls were calculated.

Trypan Blue Cell Viability Staining

Following overnight FND treatments, cells were collected and washed ×2 with phosphate-buffered saline. An aliquot of 1×10^5 cells was used for 1:1 staining with 0.4% trypan blue dye. Cells were incubated in trypan blue stain for 3 minutes and viable cells were counted using a hemocytometer.

Fluorescence Microscopy Analysis of FND Uptake

Following 24 hour FND treatments, cells were stained with PureBlu™ Hoechst 33342 Nuclear Staining Dye (Bio-Rad Laboratories, Hercules, CA). Uptake and distribution of FNDs were assessed using a Nikon A1R confocal microscope equipped with a 60× objective lens, NA 1.4 (Nikon Instruments, Melville, NY). FNDs were visualized using the 561 nm and 638 nm laser lines with corresponding 595/50 nm and 700/75 nm barrier filters. Representative images from each treatment group were prepared using the Nikon NIS Elements software (Ver. 4.30.02).

IFN-γ and TNF-α Enzyme-Linked Immunosorbent Assay (ELISA)

Following 24 hour FND treatments, cell-free culture supernatants were harvested and analyzed for levels of IFN-γ and TNF-α by ELISA (R&D Systems, Minneapolis, MN) as previously described.[34]

Animal Model

Wild-type BALB/c mice (The Jackson Laboratory) were injected subcutaneously in the right flank with 30 μg of either non-fluorescent or fluorescent nanodiamonds. Mice were imaged with using an IVIS Lumina II optical imaging system (Caliper Life Science Co., USA) after nanodiamond treatment to evaluate the ability to visualize and track the nanodiamonds. These studies were conducted under a protocol approved by Ohio State University's Institutional Animal Care and Use Committee.

Statistical Analysis

Log transformation was applied on SS intensity and MFI of each fluorescence channel evaluated by flow cytometry. FND optimal treatment dose analysis was performed using random effects mixed model and t-tests. Multiple comparisons were adjusted by Tukey's

method.[35] A linear trend test across FND treatment doses was performed. Cell viability was analyzed using random effects mixed model and F-tests were used for testing overall difference.[36] Analyses of optimal FND treatment duration, surface marker expression and cytokine production were performed using random effects mixed model and t-tests. Multiple comparisons were adjusted using Holm's method.[37] Statistical analyses were performed using SAS®9.4 software. Level of significance was set at 0.05.

RESULTS

FND Characterization

The FNDs generated in this study were uncoated, non-functionalized, and not activated. NV-centers are point defects within the diamond lattice that produce infrared fluorescence upon excitation and may be visualized via confocal microscopy. Figure 1A demonstrates the fluorescence of micron-sized diamonds' NV-centers. Similar results were obtained for nano-sized diamonds (data not shown). Upon excitation with a 532 nm laser, FND NV-centers emit broad fluorescence between ~600–800 nm with maximum fluorescence at 684 nm (Figure 1B). SEM analysis demonstrated that FNDs display non-spherical morphology (Figure 1C) with an average hydrodynamic size of 70 ± 28 nm (Figure 1D).

Optimal FND Treatment Dose

RAW264.7 cells, NKL cells, monocytes, and NK cells were cultured overnight in 10% HAB medium alone or in the presence of varying doses of FNDs (12.5–200 μg/ml). Cells were then harvested and cellular FND uptake was evaluated by flow cytometry. FNDs scatter light in the visible region and an increase in SS of FND-treated cells is indicative of cellular uptake. Further, FNDs emit fluorescence in the NIR region, and an increase in NIR fluorescence of FND-treated cells suggests FND uptake. Scatter plots were employed to examine SS by FS (to evaluate changes in cellular granularity and size, respectively) and SS by NIR (to examine variations in granularity and NIR fluorescence; shown in Figure 2A). Quadrant 2 in these plots represents double-positive cells, denoted SS^+NIR^+, which are presumed to have taken up FNDs. Fold changes in SS and NIR fluorescence, as well as percent FND uptake (percent SS^+NIR^+ cells) were quantified compared to untreated controls (Figure 2B).

FND treatment resulted in a dose-dependent increase in SS in RAW264.7 cells and NKL cells, as well as healthy donor human monocytes and NK cells. A significant increase in SS was observed for RAW264.7 cells across all treatment concentrations compared to untreated cells ($p < 0.0001$). Monocytes displayed a substantial increase in SS starting at 25 μg/ml FND treatment ($p = 0.086$), and a significant increase in SS was observed at 50 μg/ml FND ($p = 0.028$) compared to untreated controls. There was no significant difference between the 25 μg/ml and 50 μg/ml treatment doses ($p = 0.812$). NKL cells demonstrated a significant increase in SS following treatment with 25 μg/ml FND ($p = 0.036$) and NK cells displayed a significant increase in SS starting at 100 μg/ml FND treatment ($p = 0.007$).

Upon examination of NIR fluorescence (NIR MFI) in FND-treated cells, it was found that NIR MFI was increased significantly across all treatment concentrations in RAW 264.7 cells

and monocytes compared to untreated cells ($p < 0.0001$ for both). A significant increase in NIR MFI was observed upon treatment with 100 μg/ml FND in NKL and NK cells ($p = 0.007$ and 0.012, respectively). Lastly, SS^+NIR^+ double-positive cells were quantified as a measure of percent FND uptake for each cell population. Percent FND uptake was significantly enhanced across all treatment concentrations for RAW264.7 cells and monocytes compared to untreated controls ($p < 0.006$ and $p < 0.0001$, respectively). Percent FND uptake was significantly increased upon treatment with 50 μg/ml FND for NKL cells ($p = 0.006$) and at 100 μg/ml FND treatment for NK cells ($p = 0.008$). Overall, RAW264.7 murine macrophages and human monocytes displayed greater FND uptake compared to NKL and NK cells.

The optimal treatment concentrations were then selected based on the minimum FND concentration required to see a significant increase in SS, NIR MFI and SS^+NIR^+ double-positive cells. Monocytes displayed a substantial increase in SS starting at 25 μg/ml FND treatment ($p = 0.086$), and a significant increase in SS was observed at 50 μg/ml FND ($p = 0.028$) compared to untreated controls. Additionally, there was no significant difference between the 25 μg/ml and 50 μg/ml treatment doses ($p = 0.812$). NIR MFI was increased significantly across all treatment concentrations monocytes compared to untreated cells ($p < 0.0001$). Percent of SS^+NIR^+ double-positive cells was also significantly enhanced across all treatment concentrations compared to untreated controls ($p < 0.0001$). Therefore, the minimum concentration required to see a significant increase in SS, NIR MFI, and SS^+NIR^+ double-positive cells was 25 μg/ml FND. NK cells displayed a significant increase in SS starting at 100 μg/ml FND treatment ($p = 0.007$). A significant increase in NIR MFI was observed upon treatment with 100 μg/ml FND in NK cells ($p = 0.012$). The percentage of SS^+NIR^+ double-positive cells was significantly increased upon treatment with 100 μg/ml FND treatment in NK cells ($p = 0.008$). Therefore, a minimum concentration of 100 μg/ml FND was required to see a significant increase in SS, NIR MFI, and SS^+NIR^+ double-positive cells. Taken together, this data suggested that 25 μg/ml represents an effective FND treatment dose for RAW264.7 cells and monocytes, whereas 100 μg/ml represents an optimal treatment dose for NKL and NK cells.

FND Optimal Treatment Duration

Monocytes and NK cells were treated with FNDs (25 μg/ml or 100 μg/ml, respectively) for 6, 12, 24, or 48 hours. Following treatment, cells were evaluated by flow cytometry and fold changes in SS, NIR MFI, and percent FND uptake (percent SS^+NIR^+ cells) were quantified compared to untreated controls (Figure 3). Compared to untreated controls both monocytes and NK cells displayed substantial increases in SS, NIR MFI and percent FND uptake across all time points.

To identify the optimal treatment duration where maximal FND uptake is observed, comparisons between each treatment group were performed. Percent FND uptake of FND-treated monocytes was not significantly different between the 6, 12, 24, or 48 hour treatment groups. However, comparisons between each time point for FND-treated monocytes demonstrated a significant increase in SS in the 24 hour treatment group compared to the 6 hour treatment group ($p = 0.035$), indicating that 24 hours represents a reasonable monocyte

FND treatment period. Comparisons between each time point for FND-treated NK cells displayed a significant increase in percent FND uptake in the 48 hour treatment group compared to the 12 hour ($p = 0.006$) and 24 hour ($p = 0.043$) treatment groups. However, no differences in SS or NIR MFI were identified between the 24 and 48 hour time points. Thus, it was concluded that 24 hours may be considered an optimal NK cell FND treatment duration. Given that both cell types (monocytes and NK cells) demonstrated significant FND uptake at 24 hours, this time point was utilized for further analyses.

FND Localization by Fluorescence Microscopy

To confirm that FNDs were indeed taken up by immune cells and not simply adhering to the cell surface, confocal microscopy was employed to confirm the intracellular location of the FNDs. RAW264.7 cells, monocytes, NKL and NK cells were treated with FNDs for 24 hours. Cells were then imaged via confocal microscopy. Two-dimensional maximum intensity projections of the fluorescence image stacks were generated as well as cross-sectional composite images composed of the differential interference contrast and fluorescence projections. These images revealed red fluorescence emitted by FNDs contained within the cell membrane and surrounding the blue fluorescence of the stained nucleus. Therefore, confocal microscopy demonstrated FND uptake into each cell type (Figure 4). Additionally, serial sections of RAW264.7 cells treated with FNDs with confocal imaging clearly demonstrated that the nucleus appears as a central open space that was devoid of diamonds (Figure 5). Similar claims have been reported by other groups.[38–40] The diffuse FND uptake seen within the cells with no FNDs present within the nuclei on confocal imaging indicate that the FNDs taken up by the cells could certainly reside within the cytoplasm and the endosomes of the cell. In line with the observations made by flow cytometry, RAW264.7 cells and monocytes displayed greater FND uptake compared to NKL and NK cells.

FND-treated Immune Cell Viability

Next, FND biocompatibility was evaluated. Since the optimal treatment dose for healthy donor human NK cells was determined to be four-fold higher than that of monocytes, monocytes and NK cells were treated with varying doses of FNDs (12.5–200 μg/ml) for 24 hours. Subsequently, cell viability was evaluated via trypan blue staining. FND treatment resulted in no significant cell death in monocytes ($p = 0.238$) or NK cells ($p = 0.980$) across all treatment concentrations compared to untreated controls. Monocyte viability ranged from 87–95% and NK cell viability ranged from 90–92% across the untreated controls and treatment groups (Figure 6).

Immune Cell Activation by FND

FND-mediated immune cell activation was evaluated by examining changes in surface marker expression and cytokine production in FND-treated human monocytes and NK cells compared to untreated controls of each cell type. Accordingly, expression of monocyte surface markers HLA-DR and CD86 as well as NK cell markers NKG2D and CD69 were evaluated. Further, monocyte TNF-α production and NK cell IFN-γ production were measured following treatment with FNDs. It has been shown previously that NK cells require priming via stimulatory factors to achieve their full effector potential.[28] Therefore, in

order to appropriately investigate the ability of FNDs to modulate NK cell activity and to provide a positive control, NK cells were cultured in the presence or absence of the stimulatory cytokine IL-12.

No significant differences in HLA-DR or CD86 expression were observed in FND-treated monocytes compared to untreated controls ($p = 1.0$ for both; Figure 7A). NK cells treated with IL-12 alone demonstrated a significant increase in CD69 expression compared to untreated NK cells ($p = 0.032$), but no significant difference in NKG2D expression was seen ($p = 1.0$). NKG2D and CD69 expression levels were significantly increased in NK cells treated with FNDs alone compared to untreated controls ($p < 0.001$). NK cells treated with both IL-12 and FNDs also demonstrated a significant increase in NKG2D and CD69 expression compared to untreated controls ($p < 0.001$). Combined treatment of NK cells with IL-12 plus FND resulted in a greater than additive increase in CD69 expression at both the 25 μg/ml ($p = 0.032$) and 100 μg/ml FND doses ($p = 0.045$). However, this effect was not observed in regard to NKG2D expression (Figure 7B).

Upon examination of cytokine production by innate immune cells following treatment with unconjugated FNDs, FND-treated monocytes demonstrated a significant increase in TNF-α production compared to untreated controls at both the 25 μg/ml FND ($p = 0.015$) and 100 μg/ml FND treatment doses ($p = 0.007$) (Figure 7C). No difference in TNF-α production was observed for FND-treated NK cells (data not shown). FND-treated monocytes, FND-treated NK cells in the absence of IL-12, and FND-untreated NK cells in the presence of IL-12 did not display a significant increase in IFN-γ production compared to untreated controls (monocyte data not shown). However, both 25 μg/ml and 100 μg/ml FND-treated NK cells in the presence of IL-12 produced significantly more IFN-γ than those treated with IL-12 alone ($p < 0.0001$) or FNDs alone ($p < 0.0001$) (Figure 7D).

Visualization of FNDs in an Animal Model

Evaluation of the ability to detect fluorescence emission from the FNDs was conducted in an animal model. Wild-type BALB/c mice were injected subcutaneously in the right flank with 30 μg of either non-fluorescent or fluorescent nanodiamonds. After nanodiamond treatments, the mice were imaged with using an IVIS Lumina II optical imaging system to evaluate the ability to visualize and track the nanodiamonds. The FNDs were easily visualized, demonstrating that in vivo tracking of FNDs is feasible (Figure 8).

DISCUSSION

Fluorescent nanodiamonds are a new class of the carbon nanoparticle family that are nontoxic, emit bright, photostable fluorescence in the NIR region, and have emerged as a promising therapeutic agent in the field of nanomedicine, including cancer therapy.[3,6,8,18,41,42] The present study has characterized the immunologic implications of treatment with FNDs. FNDs used in this study demonstrated an average hydrodynamic size of 70 ± 28 nm and maximum photostable fluorescence at 684 nm. Unconjugated FNDs were employed to evaluate the effects of FND treatment on innate immune cells, such as NK cells and monocytes. Following treatment, phagocytic immune cells (RAW264.7 murine macrophages and human monocytes) displayed significant FND uptake. Uptake by non-

phagocytic cells (human NKL cells and NK cells) was low but measurable. This uptake was accomplished without adverse effects on cell viability. Moreover, it was observed that unconjugated FNDs produced alterations in immune cell activation following uptake as measured by increased NK cell CD69 and NKG2D surface expression and enhanced production of monocyte-derived TNF-α and NK cell-derived IFN-γ.

The present report demonstrates that treatment of innate immune cells with FNDs results in dose-dependent FND uptake and positive effects on immune cell activation with no adverse effects on cell viability. However, the mechanisms by which immune cells take up FNDs and become activated are not well understood. Previously, it has been suggested that some cell types engulf nanodiamonds via phagocytosis, while other cells may allow nanodiamond diffusion directly across the cell membrane.[38,43,44] Additionally, previous studies demonstrate that FNDs appear to enter cells through a clathrin-dependent endocytotic process which was demonstrated using chemical inhibitors like brefeldin as well as ATP poisons like vanadate.[39,40] Similar to our study, these studies used FNDs that lacked any kind of biomedical coating and presumably are non-specifically taken up by cells.[39,40] None of the FND studies that have been reported thus far, including the present study, show any entry of FNDs into the nucleus.[38–40] Immune cell activation may be triggered by the internalized FNDs or may be unrelated to uptake and result from stimulation of cell-surface receptors. In order to address these questions, further research to define the dynamics of FND uptake and determine the mechanism of immune cell activation is warranted.

Although nanodiamonds have considerable potential as immunological reagents, they are only recently beginning to see significant usage. In the past, fluorescent diamonds were used for photophysics applications and contained only a few NV-centers within the diamond crystal. However, the fluorescence of these nanodiamonds is far too low for most biological applications. Nanodiamonds can now be prepared with significant numbers of NV-centers but many of these lack functional groups/surface coatings for biomedical applications. The FNDs used in this study contains high numbers of NV-centers (approximately 35 centers per 35 nm crystal) and have functional groups for bioconjugation, which is crucial to their development as novel tools for immunotherapeutic applications.

Recently, it has been demonstrated that nanoparticle-based delivery systems may be employed to yield enhanced T cell-mediated anti-tumor activity via nanoparticle conjugation to CpG oligodeoxynucleotides, anti-TGF-β siRNA or anti-PD-L1 siRNA.[45–47] Moreover, it has been shown that nanoparticles are engulfed preferentially by phagocytic myeloid cells and may serve as a mechanism to target these cells and promote a tumor-suppressive environment.[48,49] For example, in a study by Huang *et al.*, a galactosylated cationic dextran nanoparticle-driven nucleic acid delivery system carrying CpG, anti-IL-10, and anti-IL-10 receptor oligodeoxynucleotides was utilized to target tumor-associated macrophages (TAM) to suppress their pro-tumorigenic functions and promote anti-tumor activity.[50] Employing similar myeloid cell targeting strategies in future experimentation with FNDs represents an exciting avenue of immunologic research.

FNDs offer unique advantages as myeloid-targeting nanoparticles, in that they possess an extensive, faceted architecture and uniquely emit bright, photostable fluorescence in the NIR

spectrum.[3,6,8,18,41,42] Additionally, previous *in vitro* and *in vivo* studies have demonstrated FND biocompatibility.[13–15,18,42] These characteristics have facilitated early characterization of immune cell FND uptake, and will also permit *in vivo* tracking to better understand the cellular localization and anti-tumor properties of FNDs. The faceted architecture of FNDs is of immense value, as it permits the conjugation of molecules that can serve as immune-stimulatory agents. For example, our group recently described a FND conjugation technique that may be universally applied for large-scale FND production. It was shown that polyethylene glycol may be utilized as a biocompatible surface coating, and subsequent PEGylation reactions may be employed for bioconjugation with molecules presenting a variety of functional groups.[3]

Non-fluorescent nanodiamond-mediated chemotherapy delivery systems have been developed with promising biocompatible mechanisms for enhancing chemotherapeutic efficacy, decreasing toxicities, and overcoming chemoresistance both *in vitro* and *in vivo*.[17,38,51–54] Similarly, some *in vitro* and *in vivo* studies have employed a nanodiamond and nanoplatinum mixture to demonstrate nanodiamond- and nanoplatinum-mediated dendritic cell activation, T cell proliferation, chemosensitization of a multidrug resistant human myeloid leukemia cell line and structural alteration of breast cancer cells.[43,55–57] However, the *in vivo* use of this mixture was through coating of the mixture onto cloths lining the mice cages and not through systemic administration. Additionally, FNDs have been used in a number of imaging experiments related to cancer research, ranging from immunofluorescence studies in a number of cell lines to sentinel lymph node mapping in small animals.[7,58–63] In this study, we have evaluated the ability to detect fluorescence emission from the FNDs using an animal model. The FNDs were easily visualized, demonstrating that *in vivo* tracking of FNDs is feasible. Thus, FNDs have the potential to serve as an immune drug delivery vehicle with "track and trace" capabilities. Further development of the FNDs described in this study could lead to agents with the potential for systemic administration and broad therapeutic applications.

The concept of "immunoengineering" has been put forth to suggest that conjugating immunotherapeutic agents to nanoparticles may enable more effective tumor penetration, controlled delivery of therapeutic agents and robust immune responses to cancer therapies.[64] A few groups have described nanodiamond surface functionalization as a therapeutic anti-tumor strategy. For example, Zhao *et al.* developed a nanodiamond platform with hyperbranched polyglycerol coating to evade macrophage uptake and conjugation with a RGD targeting peptide for preferential uptake by A549 cancer cells.[51] Similarly, Chu *et al.* developed a nanodiamond complex with conjugation of recombinant growth hormone for protein-targeting of the surface membrane of A549 NSCLC cells.[65] Salaam *et al.* developed a nanodiamond mediated drug delivery system to increase the specificity of doxorubicin by nanodiamond conjugation with doxorubicin and the DGEA peptide to target the $\alpha_2\beta_1$ integrins overexpressed in metastatic prostate cancers.[66] However, employing this strategy of nanodiamond conjugation for FND-mediated immunotherapy delivery has not yet been fully developed. Additionally, most of these previous reports used detonation nanodiamonds which are not fluorescent. Thus, FNDs have the potential to serve as an immune drug delivery vehicle with "track and trace" capabilities.

Although there have been significant advances in the field of cancer immunotherapy, such as the development of immune checkpoint inhibitors[67,68], tumor-immune escape and the development of immunotherapy resistance continues to pose a challenge.[19,23,25] Targeted innate immune cell activation could address these challenges and promote reversal of tumor-mediated immunosuppression to yield enhanced anti-tumor activity. This study has demonstrated that FNDs may be utilized to engage innate immune cells and potentially serve as a powerful tool for targeted immunotherapy. The versatile surface of FNDs may be conjugated to immunomodulatory agents and function as a novel mechanism to maximize immune cell activation. Thus, future studies will investigate the ability to conjugate FNDs with antibodies or other immunomodulatory agents to develop an innate immune cell targeting strategy and promote anti-tumor activity.

Acknowledgments

The authors would like to thank The Ohio State University Comprehensive Cancer Center's Analytical Cytometry Shared Resource for providing equipment used in flow cytometry analyses and the Small Animal Imaging Core at The Ohio State University for providing equipment used for animal IVIS optical imaging. Thank you to Dr. Sara Cole at the Ohio State University Microscopy and Imaging Facility for assisting in imaging, data collection, and figure preparation for confocal microscopy images. We thank the Molecular Foundry for their support and access to characterization equipment.

Funding: This work was supported by National Institutes of Health Grants P01 CA95426 (W.E.C.), T32 5T32CA090223-12 (L.P.S-K.) and P30 CA016058 and the Pelotonia Graduate Research Fellowship (A.R.C.). Development of fluorescent nanodiamonds was supported by the National Heart, Lung and Blood Institute under contract No. HHSN268201300031C (A.A.R). Work at the Molecular Foundry was supported by the Office of Science, Office of Basic Energy Sciences, of the U.S. Department of Energy under Contract No. DE-AC02-05CH11231 (M.S.W. and A.B.).

ABBREVIATIONS

Ab	antibody
APC	allphycocyanin
ELISA	enzyme-linked immunosorbent assay
FND(s)	fluorescent nanodiamond(s)
FS	forward laser light scatter
HAB	Human AB serum
HLA	human leukocyte antigen
IFN-γ	interferon gamma
mAb	monoclonal-antibody
MFI	mean fluorescence intensity
MPI	maximum intensity projections
NIR	near-infrared
NK	natural killer

NV	nitrogen-vacancy
PBMC	peripheral blood mononuclear cell
PE	phycoerythrin
SEM	scanning electron microscopy
SS	side laser light scatter
TNF-α	tumor necrosis factor alpha

References

1. Collins AT. Optical centres produced in diamond by radiation damage. New Diamond and Frontier Carbon Technnology. 2007; 17:47–61.
2. Campbell B, Choudhury W, Mainwood A, Newton M, Davies G. Lattice damage caused by the irradiation of diamond. Nuclear Instruments and Methods in Physics Research Section A: Accelerators, Spectrometers, Detectors and Associated Equipment. 2002; 476:680–5.
3. Suarez-Kelly LP, Rampersaud IV, Moritz CE, et al. Fluorescent nanodiamonds and their use in biomedical research. Proc SPIE 9762, Advances in Photonics of Quantum Computing, Memory, and Communication IX. 2016; 2016:976205–21.
4. Ho D. Beyond the sparkle: the impact of nanodiamonds as biolabeling and therapeutic agents. ACS nano. 2009; 3:3825–9. [PubMed: 20025300]
5. Krueger A. Beyond the shine: recent progress in applications of nanodiamond. Journal of Materials Chemistry. 2011; 21:12571.
6. Mochalin VN, Shenderova O, Ho D, Gogotsi Y. The properties and applications of nanodiamonds. Nat Nanotechnol. 2012; 7:11–23.
7. Vaijayanthimala V, Cheng PY, Yeh SH, et al. The long-term stability and biocompatibility of fluorescent nanodiamond as an in vivo contrast agent. Biomaterials. 2012; 33:7794–802. [PubMed: 22863379]
8. Schirhagl R, Chang K, Loretz M, Degen CL. Nitrogen-vacancy centers in diamond: nanoscale sensors for physics and biology. Annu Rev Phys Chem. 2014; 65:83–105. [PubMed: 24274702]
9. Hermanson, GT. Bioconjugate techniques. San Diego: Academic Press; 1996.
10. Krueger A, Lang D. Functionality is Key: Recent Progress in the Surface Modification of Nanodiamond. Advanced Functional Materials. 2012; 22:890–906.
11. Boudou J-P, David M-O, Joshi V, H E, Curmi PA. Hyperbranched polyglycerol modified fluorescent nanodiamond for biomedical research. Diamond and Related Materials. 2013; 38
12. Rosenholm JM, Vlasov II, Burikov SA, Dolenko TA, Shenderova OA. Nanodiamond-Based Composite Structures for Biomedical Imaging and Drug Delivery. J Nanosci Nanotechnol. 2015; 15:959–71. [PubMed: 26353602]
13. Lai L, Barnard AS. Functionalized Nanodiamonds for Biological and Medical Applications. J Nanosci Nanotechnol. 2015; 15:989–99. [PubMed: 26353604]
14. Kaur R, Badea I. Nanodiamonds as novel nanomaterials for biomedical applications: drug delivery and imaging systems. Int J Nanomedicine. 2013; 8:203–20. [PubMed: 23326195]
15. Perevedentseva E, Lin YC, Jani M, Cheng CL. Biomedical applications of nanodiamonds in imaging and therapy. Nanomedicine (Lond). 2013; 8:2041–60. [PubMed: 24279492]
16. Kossovsky N, Gelman A, Hnatyszyn HJ, et al. Surface-modified diamond nanoparticles as antigen delivery vehicles. Bioconjugate chemistry. 1995; 6:507–11. [PubMed: 8974446]
17. Chow EK, Zhang XQ, Chen M, et al. Nanodiamond therapeutic delivery agents mediate enhanced chemoresistant tumor treatment. Sci Transl Med. 2011; 3:73ra21.
18. Vaijayanthimala V, Lee DK, Kim SV, et al. Nanodiamond-mediated drug delivery and imaging: challenges and opportunities. Expert Opin Drug Deliv. 2015; 12:735–49. [PubMed: 25510332]

19. Gabrilovich DI, Ostrand-Rosenberg S, Bronte V. Coordinated regulation of myeloid cells by tumours. Nat Rev Immunol. 2012; 12:253–68. [PubMed: 22437938]
20. Shi C, Pamer EG. Monocyte recruitment during infection and inflammation. Nat Rev Immunol. 2011; 11:762–74. [PubMed: 21984070]
21. Murray PJ, Wynn TA. Protective and pathogenic functions of macrophage subsets. Nat Rev Immunol. 2011; 11:723–37. [PubMed: 21997792]
22. Marcus, A., Gowen, BG., Thompson, TW., et al. Chapter Three - Recognition of Tumors by the Innate Immune System and Natural Killer Cells. In: Frederick, WA., editor. Advances in Immunology. Academic Press; 2014. p. 91-128.
23. Kersten K, Salvagno C, de Visser KE. Exploiting the immunomodulatory properties of chemotherapeutic drugs to improve the success of cancer immunotherapy. Frontiers in Immunology. 2015; 6
24. Leibson PJ. Signal transduction during natural killer cell activation: inside the mind of a killer. Immunity. 1997; 6:655–61. [PubMed: 9208838]
25. Goldberg JL, Sondel PM. Enhancing Cancer Immunotherapy Via Activation of Innate Immunity. Seminars in Oncology. 2015; 42:562–72. [PubMed: 26320061]
26. Maecker HT, McCoy JP, Nussenblatt R. Standardizing immunophenotyping for the Human Immunology Project. Nat Rev Immunol. 2012; 12:191–200. [PubMed: 22343568]
27. Markikou-Ouni W, Drini S, Bahi-Jaber N, Chenik M, Meddeb-Garnaoui A. Immunomodulatory Effects of Four Leishmania infantum Potentially Excreted/Secreted Proteins on Human Dendritic Cells Differentiation and Maturation. PLoS One. 2015 10:DOI:10.1371 [Online November 18, 2015].
28. Vivier E, Raulet DH, Moretta A, et al. Innate or Adaptive Immunity? The Example of Natural Killer Cells. Science. 2011; 331:44–9. [PubMed: 21212348]
29. Martin-Fontecha A, Thomsen LL, Brett S, et al. Induced recruitment of NK cells to lymph nodes provides IFN-[gamma] for TH1 priming. Nat Immunol. 2004; 5:1260–5. [PubMed: 15531883]
30. Moretta A, Marcenaro E, Sivori S, Chiesa MD, Vitale M, Moretta L. Early liaisons between cells of the innate immune system in inflamed peripheral tissues. Trends in Immunology. 2005; 26:668–75. [PubMed: 16198147]
31. Boudou JP, Curmi PA, Jelezko F, et al. High yield fabrication of fluorescent nanodiamonds. Nanotechnology. 2009; 20:235602. [PubMed: 19451687]
32. Kondadasula SV, Roda JM, Parihar R, et al. Colocalization of the IL-12 receptor and FcgammaRIIIa to natural killer cell lipid rafts leads to activation of ERK and enhanced production of interferon-gamma. Blood. 2008; 111:4173–83. [PubMed: 18174382]
33. Parihar R, Nadella P, Lewis A, et al. A Phase I Study of Interleukin 12 with Trastuzumab in Patients with Human Epidermal Growth Factor Receptor-2-Overexpressing Malignancies. Clinical Cancer Research. 2004; 10:5027–37. [PubMed: 15297404]
34. Parihar R, Dierksheide J, Hu Y, Carson WE. IL-12 enhances the natural killer cell cytokine response to Ab-coated tumor cells. The Journal of clinical investigation. 2002; 110:983–92. [PubMed: 12370276]
35. Tukey JW. Comparing individual means in the analysis of variance. Biometrics. 1949; 5:99–114. [PubMed: 18151955]
36. Woolson, RF. The Partial F-Test: Tests for the Contribution of More than One Variable at the Same Time. In: Woolson, RF., Clarke, WR., editors. Statistical methods for the analysis of biomedical data. 2. New York: Wiley-Interscience; 2002. p. 559-64.
37. Holm S. A simple sequentially rejective multiple test procedure. Scand J Statistics. 1979; 6:65–70.
38. Faklaris O, Joshi V, Irinopoulou T, et al. Photoluminescent diamond nanoparticles for cell labeling: study of the uptake mechanism in mammalian cells. ACS nano. 2009; 3:3955–62. [PubMed: 19863087]
39. Perevedentseva E, Hong SF, Huang KJ, et al. Nanodiamond internalization in cells and the cell uptake mechanism. J Nanopart Res. 2013; 15:1–12.
40. Faklaris O, Garrot D, Joshi V, et al. Detection of single photoluminescent diamond nanoparticles in cells and study of the internalization pathway. Small. 2008; 4:2236–9. [PubMed: 18989862]

41. Walker J. Optical absorption and luminescence in diamond. Rep Prog Phys. 1979; 42:1605–59.
42. Yu SJ, Kang MW, Chang HC, Chen KM, Yu YC. Bright fluorescent nanodiamonds: no photobleaching and low cytotoxicity. J Am Chem Soc. 2005; 127:17604–5. [PubMed: 16351080]
43. Ghoneum M, Ghoneum A, Gimzewski J. Nanodiamond and nanoplatinum liquid, DPV576, activates human monocyte-derived dendritic cells in vitro. Anticancer Res. 2010; 30:4075–9. [PubMed: 21036722]
44. Karpukhin AV, Avkhacheva NV, Yakovlev RY, et al. Effect of detonation nanodiamonds on phagocyte activity. Cell Biol Int. 2011; 35:727–33. [PubMed: 21155712]
45. Molino NM, Neek M, Tucker JA, Nelson EL, Wang SW. Viral-mimicking protein nanoparticle vaccine for eliciting anti-tumor responses. Biomaterials. 2016; 86:83–91. [PubMed: 26894870]
46. Xu Z, Wang Y, Zhang L, Huang L. Nanoparticle-delivered transforming growth factor-β siRNA enhances vaccination against advanced melanoma by modifying tumor microenvironment. ACS Nano. 2014; 8:3636–45. [PubMed: 24580381]
47. Teo PY, Yang C, Whilding LM, et al. Ovarian cancer immunotherapy using PD-L1 siRNA targeted delivery from folic acid-functionalized polyethylenimine: strategies to enhance T cell killing. Adv Healthc Mater. 2015; 4:1180–9. [PubMed: 25866054]
48. Kourtis IC, Hirosue S, de Titta A, et al. Peripherally administered nanoparticles target monocytic myeloid cells, secondary lymphoid organs and tumors in mice. PLoS One. 2013; 8:e61646. [PubMed: 23626707]
49. Amoozgar Z, Goldberg MS. Targeting myeloid cells using nanoparticles to improve cancer immunotherapy. Adv Drug Deliv Rev. 2015; 91:38–51. [PubMed: 25280471]
50. Huang Z, Zhang Z, Jiang Y, et al. Targeted delivery of oligonucleotides into tumor-associated macrophages for cancer immunotherapy. J Control Release. 2012; 158:286–92. [PubMed: 22119956]
51. Zhao L, Xu Y-H, Akasaka T, et al. Polyglycerol-coated nanodiamond as a macrophage-evading platform for selective drug delivery in cancer cells. Biomaterials. 2014; 35:5393–406. [PubMed: 24720879]
52. Ryu TK, Lee GJ, Rhee CK, Choi SW. Cellular Uptake Behavior of Doxorubicin-Conjugated Nanodiamond Clusters for Efficient Cancer Therapy. Macromol Biosci. 2015; 15:1469–75. [PubMed: 26097075]
53. Hsieh Y-H, Liu K-K, Sulake RS, Chao J-I, Chen C. Microwave-assisted efficient conjugation of nanodiamond and paclitaxel. Bioorganic & Medicinal Chemistry Letters. 2015; 25:2074–7. [PubMed: 25890802]
54. Wang X, Low XC, Hou W, et al. Epirubicin-Adsorbed Nanodiamonds Kill Chemoresistant Hepatic Cancer Stem Cells. ACS nano. 2014; 8:12151–66. [PubMed: 25437772]
55. Ghoneum A, Sharma S, Gimzewski J. Nano-hole induction by nanodiamond and nanoplatinum liquid, DPV576, reverses multidrug resistance in human myeloid leukemia (HL60/AR). Int J Nanomedicine. 2013; 8:2567–73. [PubMed: 23888112]
56. Alia G, Huanqi Z, JungReem W, Nikita Z, Shivani S, James KG. Biophysical and morphological effects of nanodiamond/nanoplatinum solution (DPV576) on metastatic murine breast cancer cells in vitro. Nanotechnology. 2014; 25:465101. [PubMed: 25360614]
57. Ghoneum M, Ghoneum A, Tolentino L, Gimzewski J. Modulation of Aged Murine T Lymphocytes In Vivo by DPV576-C, a Nanodiamond- and Nanoplatinum-coated Material. In Vivo. 2010; 24:141–6. [PubMed: 20363985]
58. Chow EK, Zhang XQ, Chen M, et al. Nanodiamond therapeutic delivery agents mediate enhanced chemoresistant tumor treatment. Sci Transl Med. 2011; 3:73ra21.
59. Zhu Z, J L, Li W, et al. The biocompatibility of nanodiamonds and their application in drug delivery systems. Theranostics. 2012; 2:302–12. [PubMed: 22509196]
60. Mohan N, Chen CS, Hsieh HH, Wu YC, Chang HC. In vivo imaging and toxicity assessments of fluorescent nanodiamonds in Caenorhabditis elegans. Nano Lett. 2010; 10:3692–9. [PubMed: 20677785]
61. Vaijayanthimala V, Tzeng YK, Chang HC, Li CL. The biocompatibility of fluorescent nanodiamonds and their mechanism of cellular uptake. Nanotechnology. 2009; 20:425103. [PubMed: 19779240]

62. Zhang B, Li Y, Fang CY, et al. Receptor-mediated cellular uptake of folate-conjugated fluorescent nanodiamonds: a combined ensemble and single-particle study. Small. 2009; 5:2716–21. [PubMed: 19743434]

63. Zhu Y, Li W, Zhang Y, et al. Excessive sodium ions delivered into cells by nanodiamonds: implications for tumor therapy. Small. 2012; 8:1771–9. [PubMed: 22434708]

64. Goldberg MS. Immunoengineering: how nanotechnology can enhance cancer immunotherapy. Cell. 2015; 161:201–4. [PubMed: 25860604]

65. Chu H-L, Chen H-W, Tseng S-H, et al. Development of a Growth-Hormone-Conjugated Nanodiamond Complex for Cancer Therapy. ChemMedChem. 2014; 9:1023–9. [PubMed: 24677633]

66. Salaam AD, Hwang P, McIntosh R, Green HN, Jun HW, Dean D. Nanodiamond-DGEA peptide conjugates for enhanced delivery of doxorubicin to prostate cancer. Beilstein J Nanotechnol. 2014; 5:937–45. [PubMed: 25161829]

67. Sunshine J, Taube JM. PD-1/PD-L1 inhibitors. Current Opinion in Pharmacology. 2015; 23:32–8. [PubMed: 26047524]

68. Topalian Suzanne L, Drake Charles G, Pardoll Drew M. Immune Checkpoint Blockade: A Common Denominator Approach to Cancer Therapy. Cancer Cell. 2015; 27:450–61. [PubMed: 25858804]

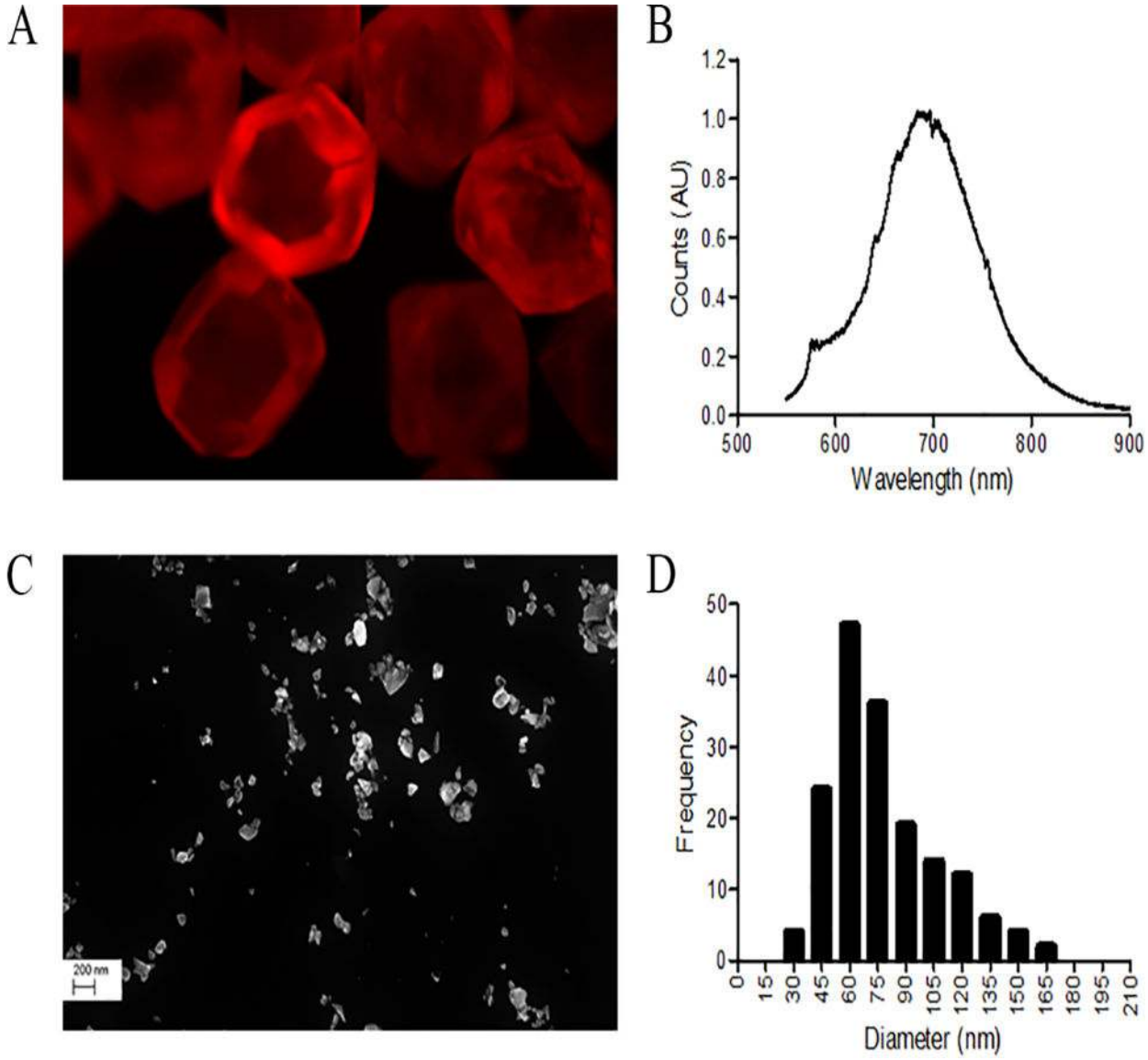

Figure 1. Characterization of FNDs

(A) Visualization of micron-sized diamonds and evaluation of nitrogen vacancy center fluorescence emission was performed using an Olympus FV1000-Filter Confocal System, employing a 543 nm laser for excitation. Maximal emission was detected between 655–755 nm. **(B)** FNDs were examined on a Horiba ARAMIS Raman microscope using a 50× objective and excited with a 532 nm laser to determine the fluorescence emission spectrum. **(C)** FND morphology was evaluated using a high resolution scanning electron microscope (SEM). **(D)** FND size (in nm) was characterized by SEM, and a frequency histogram of the particle size distribution was generated.

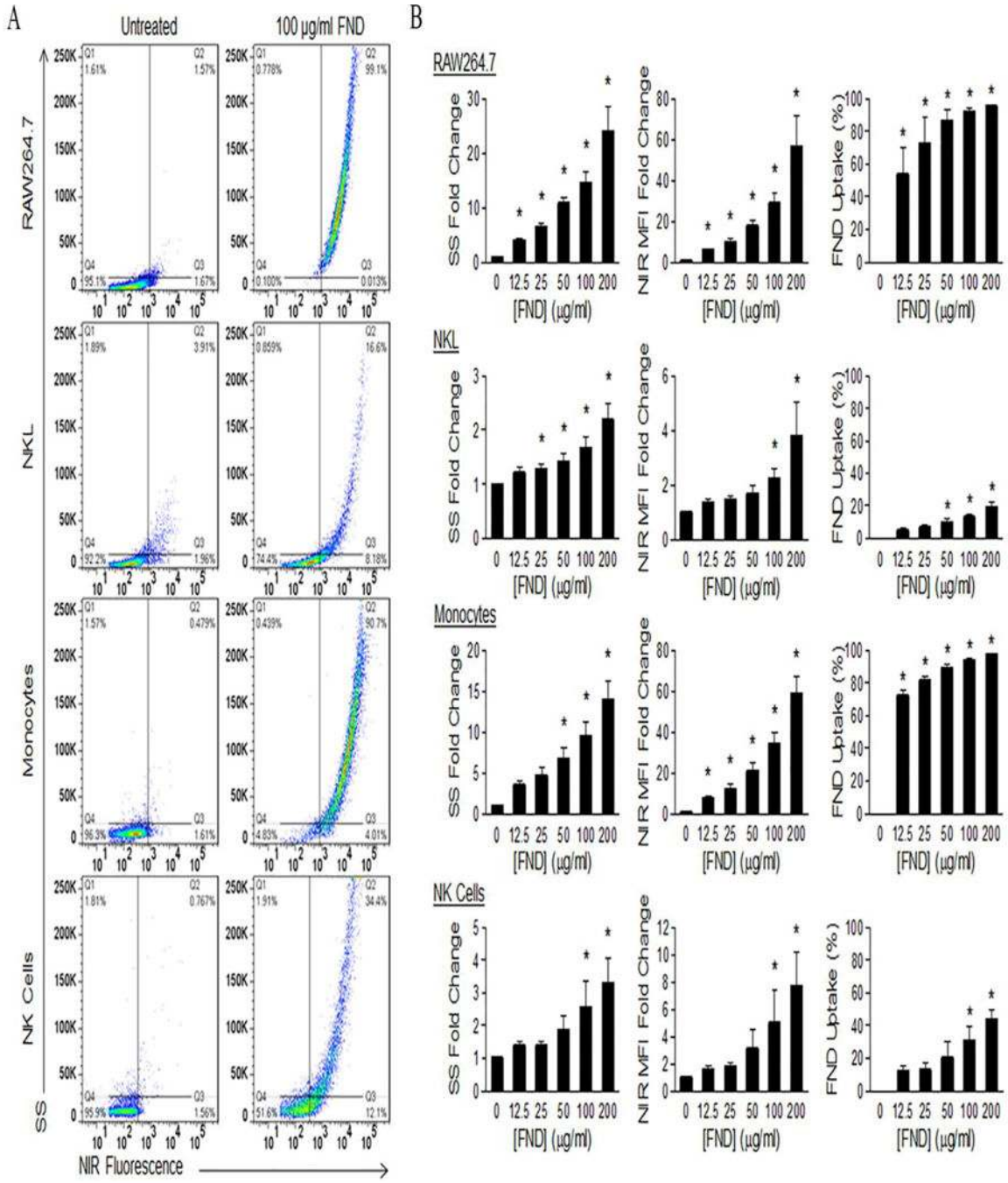

Figure 2. Analysis of FND uptake by innate immune cells

The murine macrophage cell line RAW264.7, human NK cell line NKL, and primary human monocytes and NK cells were cultured overnight in 10% HAB medium alone (untreated control, 0 µg/ml FND) or medium supplemented with increasing FND concentrations (12.5, 25, 50, 100, and 200 µg/ml). Cells then were harvested, washed, and evaluated by flow cytometry. **(A)** FND uptake was evaluated by examining shifts in immune cell side laser light scatter (SS) and near-infrared (NIR) fluorescence. $SS^{+}NIR^{+}$ double-positive cells indicate those cells that have taken up FND. **(B)** Compared to controls, fold-change in SS

(left panels) and NIR mean fluorescence intensity (MFI, middle panels) were calculated for cells treated with increasing doses of FNDs, and the percent FND uptake (measured by percent of $SS^{+}NIR^{+}$ cells) were plotted (right panels). The means ± SEM for three independent experiments are shown for all panels. Statistical analysis was performed using a random effects mixed model and t-test (* = $p < 0.05$ vs. controls).

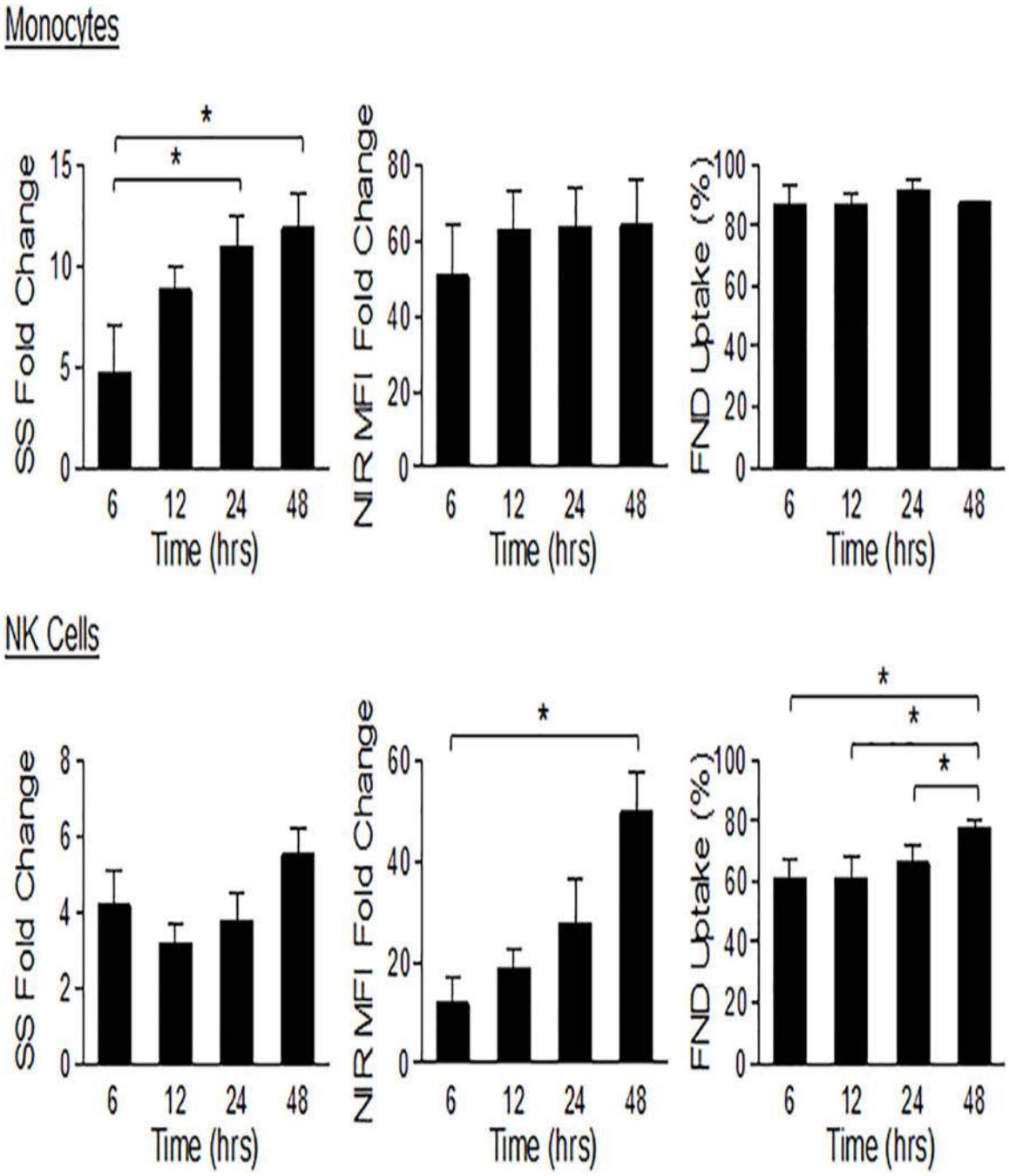

Figure 3. Time course analysis of FND uptake by primary human immune cells

Monocytes and NK cells were cultured in 10% HAB medium alone (untreated control) or medium supplemented with 25 μg/ml FND (monocytes) or 100 μg/ml FND (NK cells). Cells were cultured for 6, 12, 24, or 48 hours and then harvested, washed, and analyzed by flow cytometry. FND uptake was evaluated by examining shifts in immune cell side laser light scatter (SS, left panels) and near-infrared (NIR) mean fluorescence intensity (MFI, middle panels) as compared to untreated cells. Percent FND uptake was calculated from $SS^{+}NIR^{+}$ double-positive cells (right panels). The means ± SEM for three independent experiments

are shown for all panels. Statistical analysis was performed using a random effects mixed model, t-test, and multiple comparisons were adjusted by Holm's method (* with underlying bracket = $p < 0.05$ for comparisons among groups).

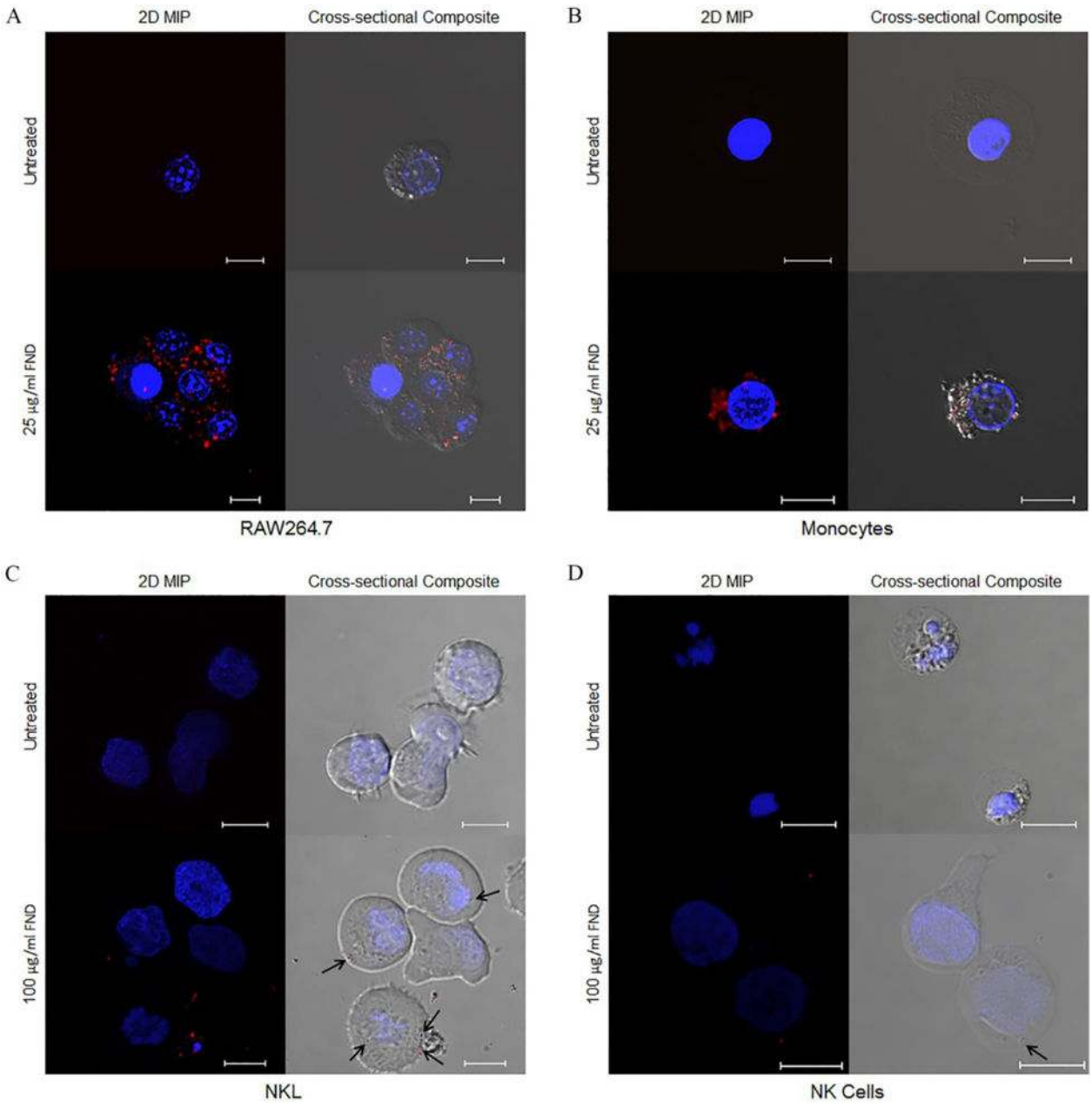

Figure 4. FNDs localize within the cytoplasm of immune cells

The murine macrophage cell line RAW 264.7, human NK cell line NKL, and primary human monocytes and NK cells were cultured for 24 hours in 10% HAB medium alone (untreated) or medium supplemented with 25 μg/ml FND (RAW264.7 and monocytes, top panels, **A** and **B**) or 100 μg/ml FND (NKL and NK cells, bottom panels, **C** and **D**). Cells were harvested, washed, and nuclei were stained using PureBlu Hoechst 33342. Image stacks were captured using a Nikon A1R confocal microscope (60× objective lens, NA 1.4). Images were captured using 402 nm, 561 nm, and 638 nm excitation lasers with collection of emission spectra from 400–750 nm. Images were analyzed using Nikon NIS-Elements AR imaging software. The dark panels located on the left of each quadrant represent a two

dimensional maximum intensity projection (MPI) of the 402 nm, 561 nm and 638 nm channels. The lighter panels on the right of each quadrant represent a cross-sectional composite image of the differential interference contrast image and the fluorescent channels. The comparison between the two images allows for localization of the FNDs within the cytoplasm of the cell. Black arrows highlight the FNDs in NKL and NK cells. Scale bar = 10 μm.

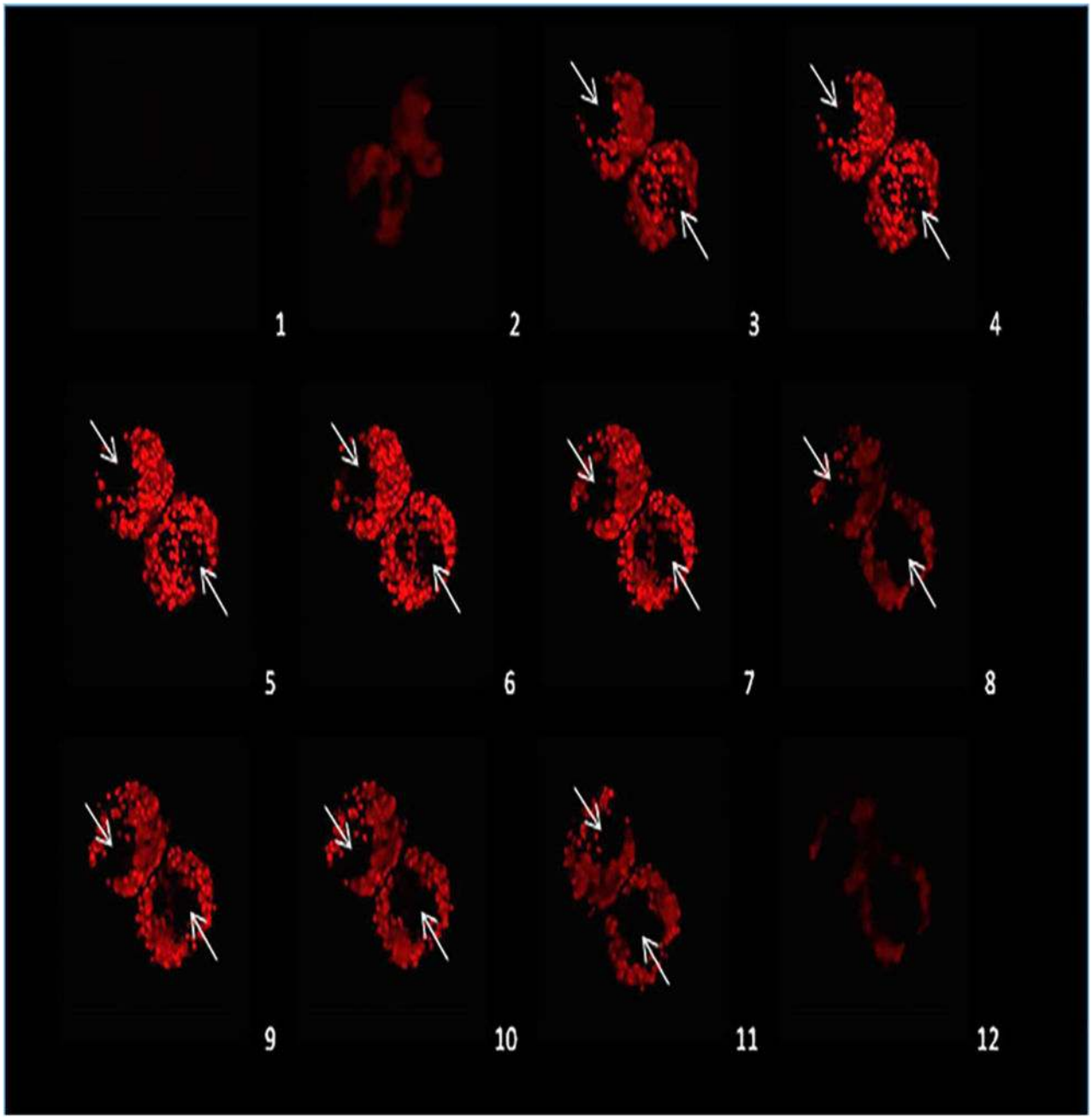

Figure 5. Serial sections with confocal imaging of FND-treated RAW264.7 cells demonstrates the nucleus as a central open space devoid of FNDs

The murine macrophage cell line RAW 264.7was cultured for 24 hours in 10% HAB medium alone (untreated) or medium supplemented with 100 μg/ml FND. Cells were then fixed with glyceraldehyde. Image stacks were captured using a Nikon A1R confocal microscope (60× objective lens, NA 1.4). Images were captured using 561 nm and 638 nm excitation lasers with collection of emission spectra from 530–750 nm. Images were analyzed using Nikon NIS-Elements AR imaging software. Serial images were obtained and each panel represents a cross-sectional composite image of the fluorescent channels. White arrows point to the cell nucleus.

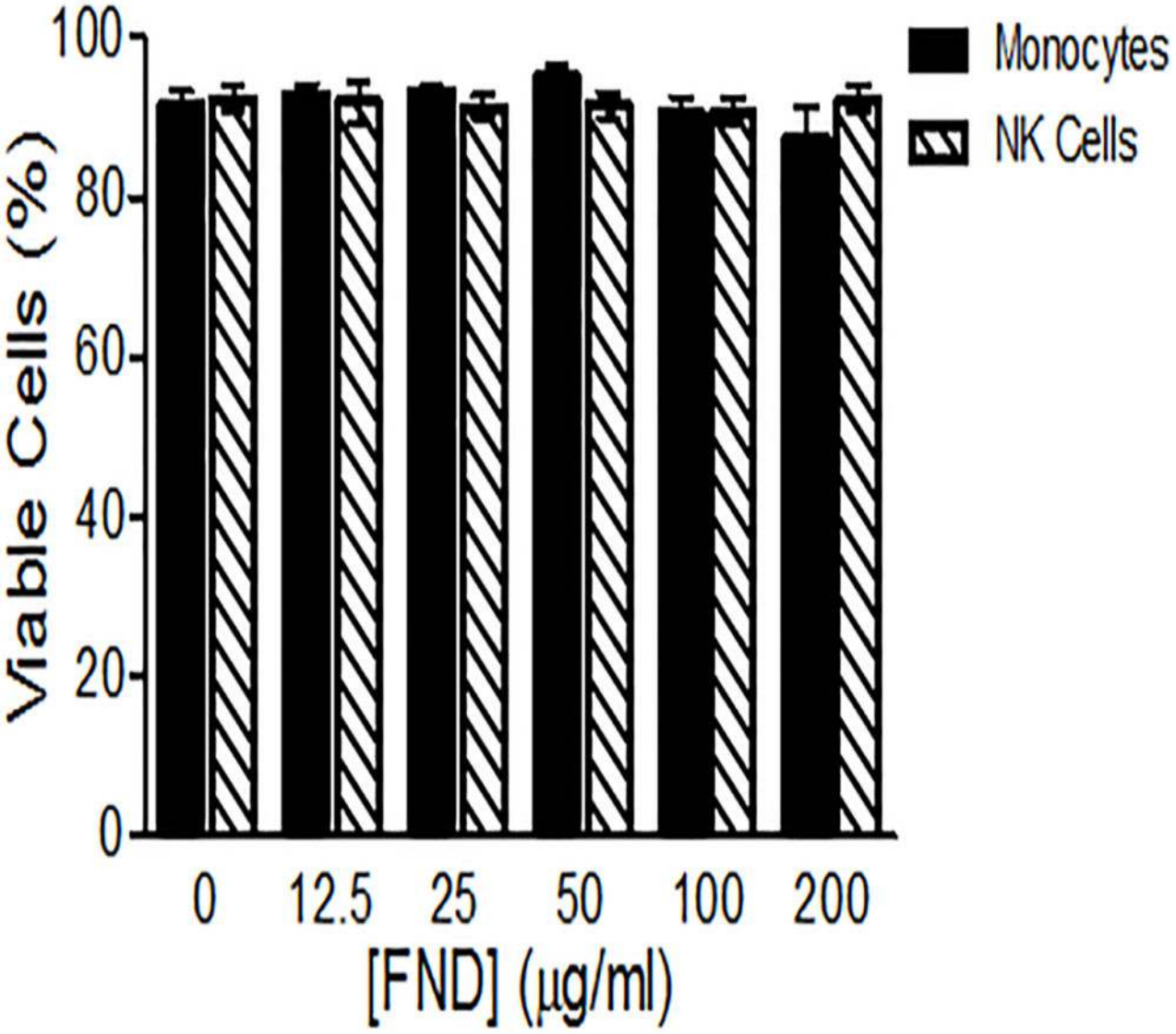

Figure 6. Treatment with FNDs does not impact immune cell viability

Primary human monocytes and NK cells were cultured for 24 hours in 10% HAB medium alone (untreated control, 0 μg/ml) or medium supplemented with increasing concentrations of FNDs (12.5, 25, 50, 100, and 200 μg/ml). Cells then were harvested, washed, and relative viability was evaluated via trypan blue dye exclusion method. Results are presented as percentage of viable cells. The means ± SEM for three independent experiments are shown.

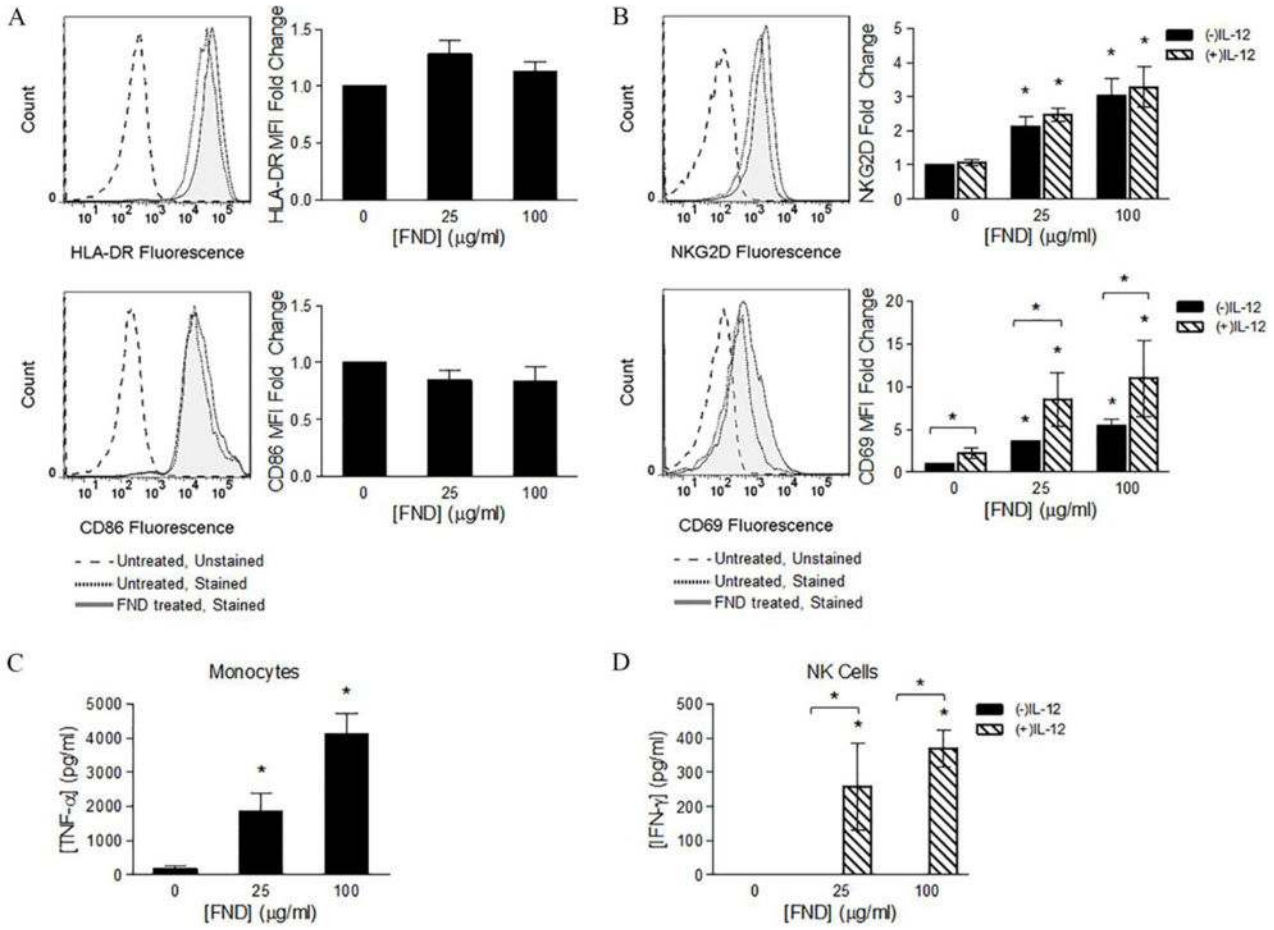

Figure 7. Treatment with FNDs promotes immune cell activation

(A) Primary human monocytes were cultured for 24 hours in 10% HAB medium alone (untreated control, 0 μg/ml FND) or medium supplemented with 25 μg/ml or 100 μg/ml FND. Cells were then harvested, washed, and stained using HLA-DR-APC mAb or CD86-PE mAb. Surface marker expression was evaluated via flow cytometry. Histograms depicting shifts in APC (top left panel) or PE (bottom left panel) fluorescence are shown. Corresponding fold-changes in mean fluorescence intensity (MFI) compared to untreated controls were calculated (right panels). **(B)** Primary human NK cells were cultured for 24 hours in 10% HAB medium alone (untreated control, 0 μg/ml FND) ± IL-12 or in medium supplemented with 25 μg/ml or 100 μg/ml FND ± IL-12. NK cells then were harvested, washed, and stained using NKG2D-APC mAb or CD69-PE mAb. Surface marker expression was evaluated by flow cytometry. Histograms depicting shifts in APC (top left panel) or PE (bottom left panel) fluorescence are shown. Corresponding fold-changes in MFI compared to untreated controls were calculated (right panels). **(C)** Cell-free supernatants from monocyte cultures were collected after 24 hours and analyzed for TNF-α production by ELISA. **(D)** Cell-free supernatants from NK cell cultures were collected after 24 hours and analyzed for IFN-γ production by ELISA. The means ± SEM for three independent experiments are shown for all panels. Statistical analysis was performed using random effects mixed model, t-test, and multiple comparisons were adjusted by Holm's method (* =

$p < 0.05$ vs. untreated controls and * with underlying bracket = $p < 0.05$ for comparisons among groups).

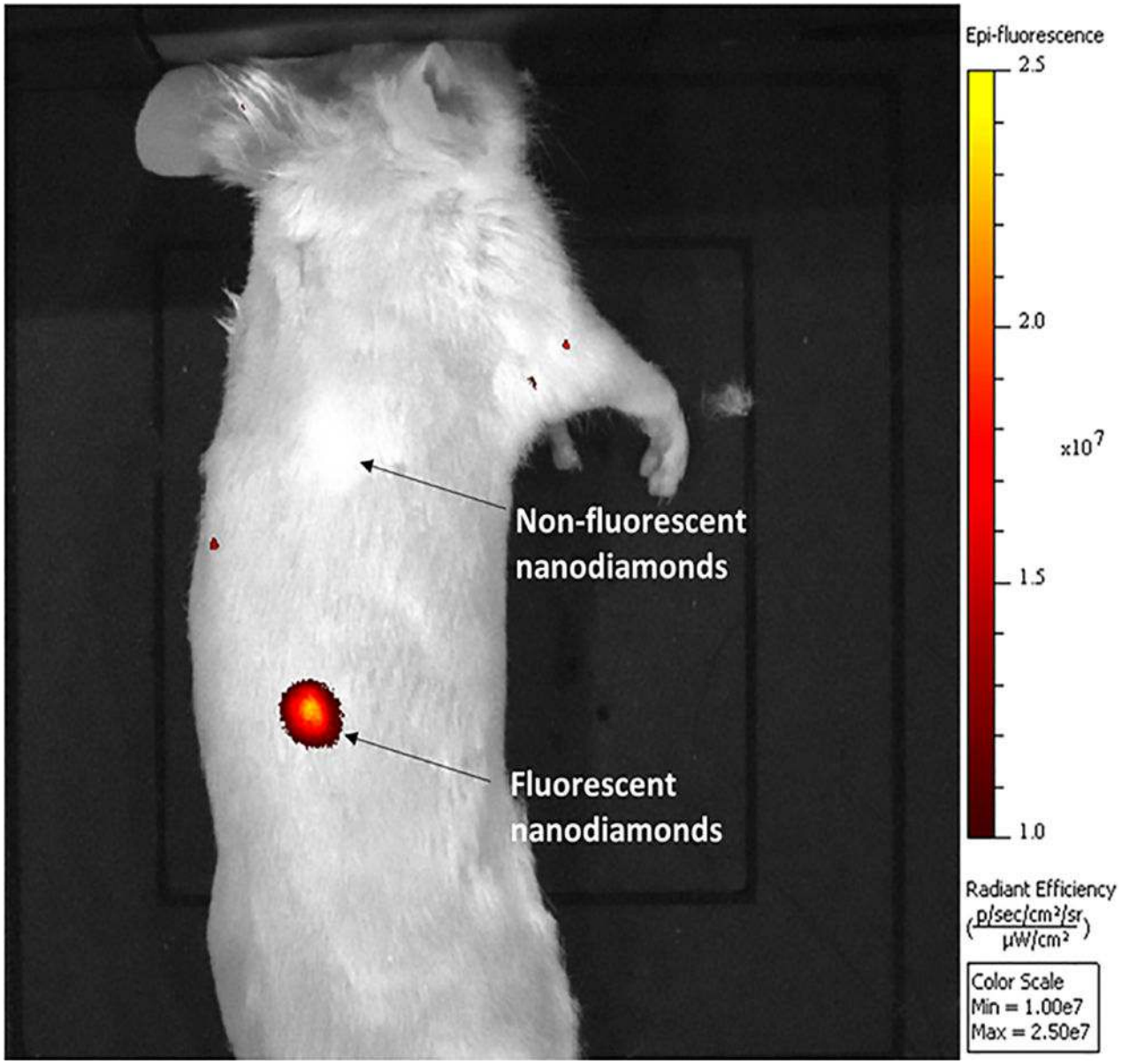

Figure 8. FNDs are easily visualized in an animal model

Wild-type BALB/c mice were injected subcutaneously in the right flank with 30 µg of either non-fluorescent or fluorescent nanodiamonds. Mice were imaged with using an IVIS Lumina II optical imaging system after nanodiamond treatment.